Severe Global Cooling After Volcanic Super-Eruptions? The Answer Hinges on Unknown Aerosol Size

ZACHARY MCGRAW,[a,b] KEVIN DALLASANTA,[a,b] LORENZO M. POLVANI,[a,c,d] KOSTAS TSIGARIDIS,[e,b] CLARA ORBE,[b,a] AND SUSANNE E. BAUER[b]

[a] *Department of Applied Physics and Applied Mathematics, Columbia University, New York, New York*
[b] *NASA Goddard Institute for Space Studies, New York, New York*
[c] *Department of Earth and Environmental Sciences, Columbia University, New York, New York*
[d] *Division of Ocean and Climate Physics, Lamont-Doherty Earth Observatory, New York, New York*
[e] *Center for Climate Systems Research, Columbia University, New York, New York*

(Manuscript received 15 March 2023, in final form 29 November 2023, accepted 1 December 2023)

ABSTRACT: Volcanic super-eruptions have been theorized to cause severe global cooling, with the 74 kya Toba eruption purported to have driven humanity to near-extinction. However, this eruption left little physical evidence of its severity and models diverge greatly on the magnitude of post-eruption cooling. A key factor controlling the super-eruption climate response is the size of volcanic sulfate aerosol, a quantity that left no physical record and is poorly constrained by models. Here we show that this knowledge gap severely limits confidence in model-based estimates of super-volcanic cooling, and accounts for much of the disagreement among prior studies. By simulating super-eruptions over a range of aerosol sizes, we obtain global mean responses varying from extreme cooling all the way to the previously unexplored scenario of widespread warming. We also use an interactive aerosol model to evaluate the scaling between injected sulfur mass and aerosol size. Combining our model results with the available paleoclimate constraints applicable to large eruptions, we estimate that global volcanic cooling is unlikely to exceed 1.5°C no matter how massive the stratospheric injection. Super-eruptions, we conclude, may be incapable of altering global temperatures substantially more than the largest Common Era eruptions. This lack of exceptional cooling could explain why no single super-eruption event has resulted in firm evidence of widespread catastrophe for humans or ecosystems.

SIGNIFICANCE STATEMENT: Whether volcanic super-eruptions pose a threat to humanity remains a subject of debate, with climate models disagreeing on the magnitude of global post-eruption cooling. We demonstrate that this disagreement primarily stems from a lack of constraint on the size of volcanic sulfate aerosol particles. By evaluating the range of aerosol size scenarios, we demonstrate that eruptions may be incapable of causing more than 1.5°C cooling no matter how much sulfur they inject into the stratosphere. This could explain why archaeological records provide no evidence of increased human mortality following the Toba super-eruption. Further, we raise the unexplored possibility that the largest super-eruptions could cause global-scale warming.

KEYWORDS: Paleoclimate; Climate models; Climate variability; Aerosol radiative effect; Volcanoes

1. Introduction

Volcanic impacts on climate have been implicated in the Roman Republic's decline and political upheavals in ancient Egypt (McConnell et al. 2020; Manning et al. 2017), among other crises Yet seen from longer time scales, the largest eruptions of recent millennia could be considered modest. Compared to the largest Common Era eruptions, super-eruptions inject into the stratosphere many times more sulfur that forms sunlight-blocking aerosol particles. This has been theorized to cause catastrophic consequences on climate (Rampino and Self 1992; Robock et al. 2009) and human populations (Ambrose 1998; Rampino and Ambrose 2000). However, knowledge of these eruptions and their impacts is limited, as no super-eruption has occurred since the one at Lake Taupo in New Zealand 25 400 years ago (Vandergoes et al. 2013). Here we use models and proxies to constrain super-eruption temperature response as much as is possible with this limited knowledge.

The most studied and debated super-eruption occurred at the site of Lake Toba in Indonesia ~74 000 years ago. This Youngest Toba eruption has been linked to a shift in glacial cycles (Rampino and Self 1992) and the potential near-extinction of humanity, possibly influencing human development (Ambrose 1998). For such extreme impacts, the Toba eruption would need to have caused global cooling many times stronger than the ~0.3°C impact of the much smaller but relatively well-observed 1991 eruption of Mt. Pinatubo (Zanchettin et al. 2022). This might be expected given Toba's injection mass of 70–6600 Tg sulfur dioxide (SO_2) gas into the stratosphere (Black et al. 2021) compared to Pinatubo's 18.4 ± 4.5 Tg SO_2 (Guo et al. 2004). Stratospheric SO_2 undergoes chemical reactions and condenses into liquid aerosol droplets that are primarily composed of sulfuric acid (hereafter referred to as *sulfate aerosol*, *sulfate particles*, or simply *aerosol*). An extreme injection of stratospheric sulfur is expected to form a dense layer of sulfate that reflects considerable sunlight. However, efforts to identify a strong temperature change contemporaneous with the Toba eruption have proved elusive. Notably, attempts to link fluctuations in ice core

Corresponding author: Zachary McGraw, zachary.mcgraw@columbia.edu

DOI: 10.1175/JCLI-D-23-0116.1

temperature proxies to Toba's occurrence have been inconsistent with an attribution to volcanic cooling (Svensson et al. 2013; Crick et al. 2021). Although a millennium-scale cooling was identified in ice core $\delta^{18}O$ records in close temporal proximity to the eruption (Zielinski et al. 1996), this was later found to be incompatible with simulations showing Toba's impacts to end within a few decades of the eruption (Robock et al. 2009). Further drawing into question the Toba eruption's severity, sites where Toba's tephra layer was identified have evidenced continuous life across the eruption. Archaeological excavations in northern India and South Africa have revealed continuous human settlement (Petraglia et al. 2007; Clarkson et al. 2020; Smith et al. 2018). Additionally, analysis of Lake Malawi biota found little change in post-eruption sediment composition (Lane et al. 2013; Yost et al. 2018). Claims of Toba's catastrophic impact are hence not substantiated by the available evidence.

Given the inability to use climate proxies to estimate cooling following super-eruptions, evaluations have relied on global climate model simulations (Rampino and Self 1992; Robock et al. 2009; Timmreck et al. 2010; Brenna et al. 2020; Osipov et al. 2020; Black et al. 2021). This represents a bottom-up approach whereby volcanic SO_2 mass estimates from sulfate deposited in ice cores (e.g., Toohey and Sigl 2017) are input to climate models that then simulate the radiative forcings of the resulting sulfate layer and the associated climate responses. Contemporary studies of Toba (Black et al. 2021; Timmreck et al. 2010; Osipov et al. 2020; English et al. 2013) have relied on *interactive aerosol models*, which include the chemical reactions that form sulfate from volcanic SO_2 gas and the microphysics of the sulfate layer's formation and decay. The transition from early modeling studies (Rampino and Self 1992; Robock et al. 2009) to interactive aerosol simulations has resulted in consensus around a reduced cooling estimate. This reduction has been attributed to more realistic prediction of volcanic aerosol size when simulating aerosol microphysical processes (Timmreck et al. 2010). However, despite considerable technical advances over the last decades, interactive aerosol model estimates of global cooling have continued to widely disagree. Even for tropical super-eruptions of similar SO_2 mass, estimates have ranged from extreme (>8°C) (Robock et al. 2009; Osipov et al. 2020) to more modest (2°–4°C) global surface cooling (Black et al. 2021; Timmreck et al. 2010).

Simulations have revealed that sulfate aerosol size increases with injection mass, and that this aerosol size enhancement limits solar reflectance and post-eruption cooling (Pinto et al. 1989; Timmreck et al. 2010). However, actual sulfate aerosol sizes following very large eruptions remains unknown, as no eruption emitting more SO_2 than Pinatubo (1991) has been observed with modern methods. Aerosol size cannot readily be estimated from ice cores, as preserved sulfate has undergone mixing and compaction that makes it unrepresentative of stratospheric aerosols. Even post-Pinatubo sulfate aerosol size is uncertain, as in situ measurements were taken at a limited number of locations (Deshler 1994; Deshler et al. 1997; Goodman et al. 1994) and flight trajectories (Pueschel et al. 1994; Wilson et al. 1993). Global-scale reconstructions of post-Pinatubo aerosol size tend to be approximations based on satellite aerosol extinction retrievals (Bingen et al. 2004; Thomason 1992), with no substantial record of larger injection cases.

Since no observations of super-eruption aerosol size exist, estimates rely on empirical relationships or model process representations. To simplify our discussion of aerosol size, we will focus on the area-weighted radius of the aerosol size distribution, a standard metric known as *effective radius* (R_{eff}) (Hansen and Travis 1974). We will especially discuss its maximum global mean value reached after the eruptions, which we refer to as *peak* R_{eff}. Compared to the peak R_{eff} near 0.55 μm that followed Pinatubo's 1991 eruption (Sato et al. 2012), the peak R_{eff} that follows eruptions injecting more stratospheric mass could theoretically vary between two bounds. These represent minimal aerosol size, with all injected sulfur mass beyond that of Pinatubo forming new aerosols to keep peak R_{eff} constant near 0.55 μm, and maximal aerosol size, with all additional sulfur mass depositing onto the same number of aerosols as had formed after Pinatubo.

Simple estimates treat the size of sulfate aerosols as increasing with injected mass via a power-law scaling (Toohey et al. 2016; Crowley and Unterman 2013)

$$R_{\text{eff}} \propto (M_{\text{SO}_2})^k, \tag{1}$$

where the constant k dictates the increase in sulfate aerosol size from one injected mass (M_{SO_2}) to another, and is bounded between the unchanging aerosol size case (at $k = 0$) and the maximal aerosol size increase case (at $k = 1/3$). This power-law scaling is used to capture the complex microphysical interactions in a highly approximated form. More specifically, for a generic eruption (i) with Pinatubo as a reference case, the scaling law takes the form

$$R_{\text{eff},i} = R_{\text{eff,Pinatubo}} \times (M_{\text{SO}_2,i}/M_{\text{SO}_2,\text{Pinatubo}})^k. \tag{2}$$

While it has already been established that large sulfate aerosol particle size reduces the surface cooling from super-eruptions (Timmreck et al. 2010), this effect has not been explored beyond individual uses of a single climate model. In this study we compare prior model studies of large eruptions and show that these have been unable to effectively constrain aerosol size. We then demonstrate that the spread in aerosol size among modeling studies is the main reason behind the spread in post-eruption cooling magnitude. By exploring the physical limits of volcanic aerosol size, we show that current knowledge is too limited for super-eruption temperature impacts to be well constrained. We evaluate the scaling between eruption mass and aerosol size in an interactive aerosol model, and test the compatibility of aerosol size scenarios with the available data left by extremely large eruptions. We put forward two unexplored possibilities that appear in our simulations: (i) volcanic global cooling might be unable to exceed 1.5°C no matter how much SO_2 is injected, and (ii) global-scale warming may be a plausible response to the very largest eruptions.

2. Methods

a. Interactive volcanic aerosol simulations

To assess the scaling between injected sulfur mass and peak sulfate aerosol size, simulations were carried out with GISS ModelE2.1 coupled to the MATRIX interactive aerosol chemistry and microphysics module (Bauer et al. 2008, 2020).

MATRIX includes representations of the processes controlling volcanic aerosol size, among which sulfate-on-sulfate coagulation, new aerosol formation, and condensation of SO_2 gas onto pre-existing aerosols are most critical (Kremser et al. 2016). ModelE2.1 has 40 vertical levels extending from the surface to 0.1 hPa. Compared to the default version of ModelE2.1 with MATRIX, our simulations also include aerosol and SO_2 impacts on photolysis along with the SO_2 greenhouse effect (Osipov et al. 2020). To correct for sulfate aerosols being too small relative to Pinatubo (see Fig. 1) we also added coagulation enhancement by Van der Waals forces using a parameterization (Chan and Mozurkewich 2001) incorporated in previous studies (English et al. 2013; Sekiya et al. 2016). Since a 13 Tg SO_2 volcanic eruption with MATRIX closely matches Pinatubo observations (Fig. 1), all mass injections input into MATRIX were scaled such that the 13 Tg SO_2 injection represents an 18 Tg SO_2 Pinatubo eruption. This difference between injected and observed stratospheric sulfur mass could reflect either that much of the emitted sulfur did not reach the stratosphere (Ukhov et al. 2023) or that processes removed sulfur shortly after the eruption (Mills et al. 2016). In our ModelE2.1 eruption simulations, SO_2 is released between 20 and 26 km over the equator. We also coinject 10 Tg H_2O (Tg SO_2)$^{-1}$ to account for direct stratospheric injection of water vapor by the eruptions (Sioris et al. 2016).

b. *Prescribed volcanic aerosol simulations*

To evaluate post-eruption radiative forcings and the accompanying surface temperature responses, we have performed and analyzed a large number of simulations with prescribed aerosols. Compared to the interactive aerosol model version described above, the prescribed aerosol configuration allows greater flexibility for testing an extensive range of injected sulfur masses and sulfate aerosol sizes. For this task, the GISS ModelE2.2 climate model (Orbe et al. 2020) was used. ModelE is a high-top model with 102 vertical levels up to 89 km, and more realistically simulates stratospheric circulation than the lower vertical resolution ModelE2.1 (Orbe et al. 2020). The model was set up as in a recent study (DallaSanta and Polvani 2022), with a coupled prognostic ocean and noninteractive chemistry, although we here use unique volcanic inputs as described in the next paragraph.

Aerosol extinction and R_{eff} time series were derived from the Easy Volcanic Aerosol (EVA) module (Toohey et al. 2016) and rescaled to various combinations of injection SO_2 mass and volcanic aerosol size. This method of scaling Pinatubo-based aerosol properties simplifies interpretation of results and reduces computational expense compared to using an interactive aerosol model for all experiments. EVA has been employed by the Volcanic Model Intercomparison Project (Zanchettin et al. 2016) and offers a self-consistent framework for testing the impact of varying eruption parameters. First, we used EVA to produce aerosol extinction and size values for an 18 Tg SO_2 Pinatubo-like equatorial eruption, with default values used for remaining input parameters. EVA's fittings are based on aerosol observations of Pinatubo's 1991 eruption, so the spatiotemporal variability of all our aerosol inputs approximately replicates this eruption. To represent distinct injection masses, we then rescaled

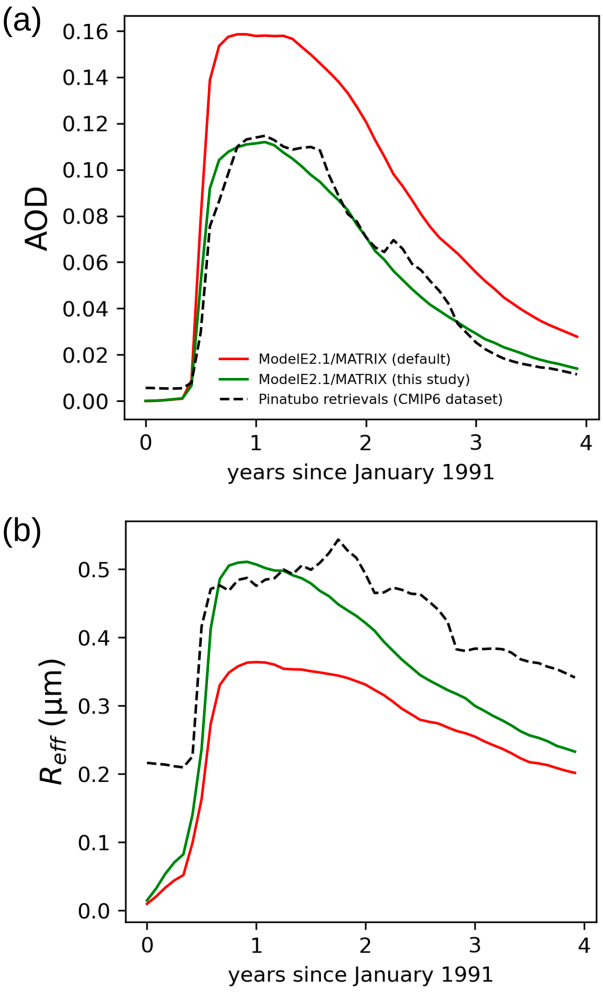

FIG. 1. Simulation of Pinatubo with GISS ModelE's interactive aerosol model. Evolutions of global mean (a) stratospheric aerosol optical depth (AOD) at 550 nm and (b) sulfate effective radius (R_{eff}) from ModelE/MATRIX simulations of a June volcanic eruption injecting 13 Tg SO_2 into the stratosphere at the location of Mt. Pinatubo. Shown is the MATRIX setup used herein (green lines) and prior to the addition of Van der Waals coagulation enhancement (red lines). The satellite-derived volcanic dataset (IACETH 2017) used in CMIP6 is shown for comparison (dashed lines). The R_{eff} values shown are globally and vertically weighted by aerosol extinction to avoid representing locations lacking aerosols.

the Pinatubo-based extinction and size values from EVA to a range of eruption masses up to 2000 Tg SO_2. First, we multiplied extinction values by the new injection mass divided by 18 Tg SO_2. We next rescaled the sulfate aerosol size to distinct scenarios between the bounds of zero and maximal aerosol size increase ($k = 0$ and $k = 1/3$, respectively), resulting in 28 mass–size combinations. Along with the size rescaling, extinction values were altered to preserve the theoretical relationship $M_{SO_4} \propto \text{Extinction} \times R_{\text{eff}}$ (Clyne et al. 2021) while assuming sulfate and SO_2 vary proportionally. A limitation of our prescribed aerosol setup is that it does not account for nonlinearities in the gravitational settling of aerosols,

which may reduce the aerosol extinction for the largest eruptions and limit plausible aerosol size scenarios to a narrower range than we explore (discussed further in section 7).

The resulting aerosol extinction and size values were used as input to simulate eruptions across the two-dimensional M_{SO_2}–peak R_{eff} eruption parameter space under preindustrial conditions. Peak temperature responses and aerosol radiative forcings were then output from the model, and were interpolated to cover the full mass-size space using a radial basis function method (*scipy.interpolate.Rbf* in Python). The radiative forcings were calculated using multiple radiation calls in the coupled runs, rather than in separate fixed-SST runs, and hence do not include rapid adjustments. For these simulations, all eruptions were set for 15 January of the first simulated year, as our separate analysis of specific eruption cases (described below) found little influence of eruption season on peak temperature response. To isolate the effect of aerosol size, the eruptions start from identical initial conditions. The response is defined with respect to the corresponding control run and smoothed with a 12-month moving average. With this procedure, sample uncertainty in the peak value is on the order of 0.1 K, based on analysis of the large ensembles in DallaSanta and Polvani (2022).

We also used this model setup to produce ensembles for two case studies, described in sections 5 and 6. The first is the Toba super-eruption, while the second is the largest eruption available in tree ring reconstructions, that of Mt. Samalas in AD 1257. Distinct ensemble members were produced by initializing experiments from different ENSO-neutral conditions in the long control run used by DallaSanta and Polvani (2022).

c. *Proxy temperature reconstructions*

To constrain how sulfate aerosol size scales with injection mass, we assessed whether simulations from the abovementioned Samalas ensemble are consistent with tree ring temperature reconstructions of this eruption. For this, temperature reconstructions of the years following the AD 1257 eruption (Guillet et al. 2017; Wilson et al. 2016; Schneider et al. 2015) were compared to simulations as in a previous study (Wade et al. 2020). As these proxies best represent Northern Hemisphere land during boreal summer, we compared these with June–August (JJA) simulation output averaged over land >40°N only. We additionally use reconstruction NH1 of Stoffel et al. (2015). While the proxy reconstructions all indicate that a cooling likely followed the Samalas eruption, temperature reconstructions disagree on this cooling's magnitude and whether it peaked in the first or second post-eruption summer. Second summer peaks may indicate a biological memory lag issue in the tree ring data (Zhu et al. 2020). A caveat of our model–proxy comparison is that the uncertainties are not fully comparable, since proxy records report instrumental uncertainties while model uncertainties represent climate system variability (Wade et al. 2020; Zhu et al. 2020).

3. Sulfate aerosol size following super-eruptions

We start by exploring what range of sulfate aerosol sizes are plausible after a super-eruption, and whether interactive aerosol models are useful for bounding this further. The above-described theoretical space between minimal and maximal aerosol size as a function of injection mass is illustrated by the gray shaded area in Fig. 2. Here values are extrapolated from Pinatubo, and we allow for a ±0.10 μm uncertainty to Pinatubo's 0.55 μm peak R_{eff} value. This forms the shaded range between a constant 0.45 μm R_{eff} and a $k = 1/3$ scaling starting from 0.65 μm at Pinatubo's mass.

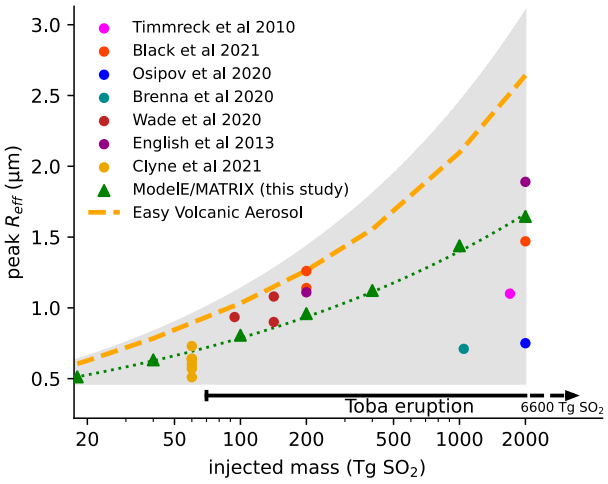

FIG. 2. Modeled sulfate aerosol size for eruptions larger than Pinatubo, showing peak global mean sulfate aerosol sizes from interactive aerosol model simulations plotted by injected mass of sulfur dioxide (SO_2). Circles represent simulations from prior studies while triangles are this study's results using ModelE/MATRIX. Also shown is a power-law fitting to the ModelE/MATRIX values (green dotted line) and output from Easy Volcanic Aerosol (orange dashed line). ModelE and EVA values were globally (and for ModelE vertically) weighted by aerosol extinction to avoid representing areas lacking sulfate. This results in a slight mismatch between the EVA values here and those presented in Toohey et al. (2016). Other R_{eff} values are shown as weighted and presented in the cited studies.

We start by assessing aerosol size agreement among past modeling studies that use interactive aerosol microphysics and chemistry to assess eruptions larger than Pinatubo (Black et al. 2021; Timmreck et al. 2010; Brenna et al. 2020; Osipov et al. 2020; Clyne et al. 2021; Wade et al. 2020; English et al. 2013). From the text and figures in these studies, we compiled the injected SO_2 masses and resulting peak global mean R_{eff} values. Information on the models used and eruptions simulated is summarized in Table 1. Note that one of these studies (Wade et al. 2020) contained simulations representing four eruption scenarios, yet two of these (LO-HAL and LO-SO2) had nearly identical results, which we averaged together and treat as a single experiment. Note also that one of these studies (Clyne et al. 2021) had output from several models, while the others each assessed one model only.

Among the assessed interactive aerosol simulations, we find no consensus on peak sulfate aerosol size following large eruptions. The peak effective radius values in these studies (plotted as circles in Fig. 2) span much of the range between the two extreme theoretical scenarios described above. Among 2000 Tg SO_2

TABLE 1. Eruption setups in prior studies that simulate large eruptions with aerosol interactive models and report sulfate aerosol size evolution. Also shown are the model setups used in this study, which includes simulations both with and without an aerosol interactive model. Asterisks denote studies that do not report surface temperature responses.

Study	Model(s)	Simulated eruption(s)	Injected SO_2 mass (Tg)	Co-injected species	Eruption month	Injection height	Injection latitude (°N)
Timmreck et al. (2010)	MAECHAM5/HAM and MPI ESM	Toba (74 kya)	1700	None	June	Unspecified	Unspecified tropical
Brenna et al. (2020)	CESM-WACCM6	Los Chocoyos (84 kya)	1046	HCl and HBr	January	24 km	14.6°N
Wade et al. (2020)	HadGEM3-ES	Samalas (1257)	95, 142	None, HCl, and HBr	June	19–34 km	−8.5°N
Osipov et al. (2020)	GISS ModelE2.1	Toba	2000	None	January	10–50 hPa (~20–30 km)	−20° to 20°N
Black et al. (2021)	CESM-WACCM4	Toba	200, 2000	None	Four-season composite	18–25 km, 35–40 km	−1.9° to 13.3°N
English et al. (2013)*	CESM-WACCM3	10x Pinatubo (1991), Toba	200, 2000	None	June	15.1–28.5 km	−2° to 14°N
Clyne et al. (2021)*	UM-UKCA, CESM-WACCM, MAECHAM5-HAM, SOCOL-AER, LMDZ-S3A	Tambora (1815)	60	None	April	22–26 km	0°
This study's interactive aerosol simulations	GISS ModelE2.1 with MATRIX	Various hypothetical eruptions	18, 40, 100, 200, 400, 1000, 2000	10 times H_2O per SO_2 mass	January	20–26 km	0°
This study's prescribed aerosol simulations	GISS ModelE2.2	Toba, Samalas, various hypothetical eruptions	18, 40, 100, 120, 200, 400, 1000, 2000	N/A (observed Pinatubo case)	January and July (Toba), July (Samalas), else January	Set by EVA (based on Pinatubo)	0°

Toba experiments, peak global mean R_{eff} values vary from 0.75 μm (Osipov et al. 2020) to 1.87 μm (English et al. 2013). This reveals that interactive aerosol models are subject to considerable uncertainties in microphysical and chemical process rates. Further, there are reasons to doubt that the spread across models in Fig. 2 represents the actual aerosol size uncertainty. First, model diversity is severely lacking. Of the six studies we compiled with eruptions $>$ 150 Tg SO_2 (including this one), five use either CESM/WACCM or ModelE. Second, we have limited confidence that models represent all relevant microphysics. Previously, a lack of Van der Waals coagulation enhancement was found to bias simulations toward small aerosol sizes (English et al. 2013). With no observations to validate simulated aerosol size following very large eruptions, we are unsure whether simulated microphysics has missing processes or biases shared across models. We hence consider the theoretical boundaries ($k = 0$ to $k = 1/3$) as spanning the range currently worth considering, rather than merely the intermodel spread.

As described above, aerosol size is expected to scale with injected mass following a particular curve. While a power-law scaling [Eq. (1)] is a common assumption, we are aware of only one study that tested this relationship with interactive aerosol models (Aubry et al. 2020), and no study that specifically compared different eruption realizations (rather than different months within simulations) or included injection masses $>$ 100 Tg SO_2. Therefore, to test the validity of the power-law functional form we ran GISS ModelE with the MATRIX interactive aerosol model (Bauer et al. 2008, 2020) over a wide range of SO_2 injection masses. Our results confirm that a power law emerges, with peak global mean effective radius values (green triangles in Fig. 2) closely following a $k = 1/4$ power-law fitting to injected mass (dashed green line in Fig. 2). This close match suggests that the power-law form is appropriate. There may exist nonlinearities in aerosol microphysics and removal processes that reduce the accuracy of a power-law scaling, especially if considering aerosols of sizes too large to stably be suspended in the stratosphere. However, as these were not encountered in our ModelE/MATRIX simulations we do not consider functional forms other than that of a power law. To the extent that the models in Fig. 2 (see circles) also follow a power law and replicate the Pinatubo eruption, the intermodel R_{eff} disagreement suggests disagreement in k. Overall, our analysis of prior interactive model studies shows little confidence in these models' ability to constrain aerosol size, although our ModelE results support the power-law scaling as a valid functional form.

4. Global surface temperature response to super-eruptions

Next, we systematically explore the extent to which this uncertainty in sulfate aerosol size causes uncertainty in post-eruption surface cooling. We accomplish this by running the GISS ModelE climate model over the potential range of aerosol sizes for injections varying from that of Pinatubo up to 2000 Tg SO_2 (the actual runs are shown as dark gray dots in Fig. 3a, with interpolation used to cover the space). For this

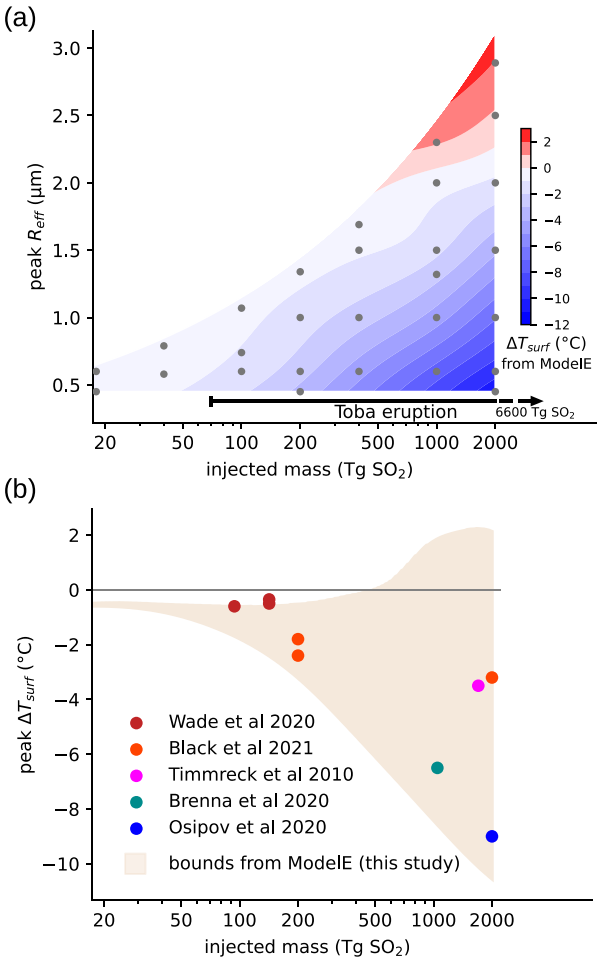

FIG. 3. Modeled post-eruption surface temperature anomalies for eruptions larger than Pinatubo, showing (a) peak global mean temperature responses from ModelE as a function of sulfate aerosol size and injection mass and (b) the range of peak surface temperature responses in the ModelE simulations compared to values from the prior studies.

we used the high-top version of GISS ModelE (Orbe et al. 2020; Rind et al. 2020) in a non-interactive-aerosol model, as this allows us to prescribe a wide range of aerosol size and injection mass scenarios. Our model runs demonstrate that the uncertainty in aerosol size alone leads to a vast breadth of peak global surface temperature responses (contour colors in Fig. 3a). For eruption masses on the order of Pinatubo, the influence of aerosol size on peak surface temperature is modest. For a Toba-scale eruption of 2000 Tg SO_2, however, our simulations show the spread to be huge: from ~11 K cooling to ~2 K warming.

We now explain the physical mechanism underlying the sensitivity of super-eruption temperature response to sulfate aerosol size. This can be understood from the sulfate's interactions with solar (shortwave) and terrestrial (longwave) radiation (Fig. 4). Greater sulfur mass results in denser sulfate plumes that reflect more sunlight, although increases in aerosol

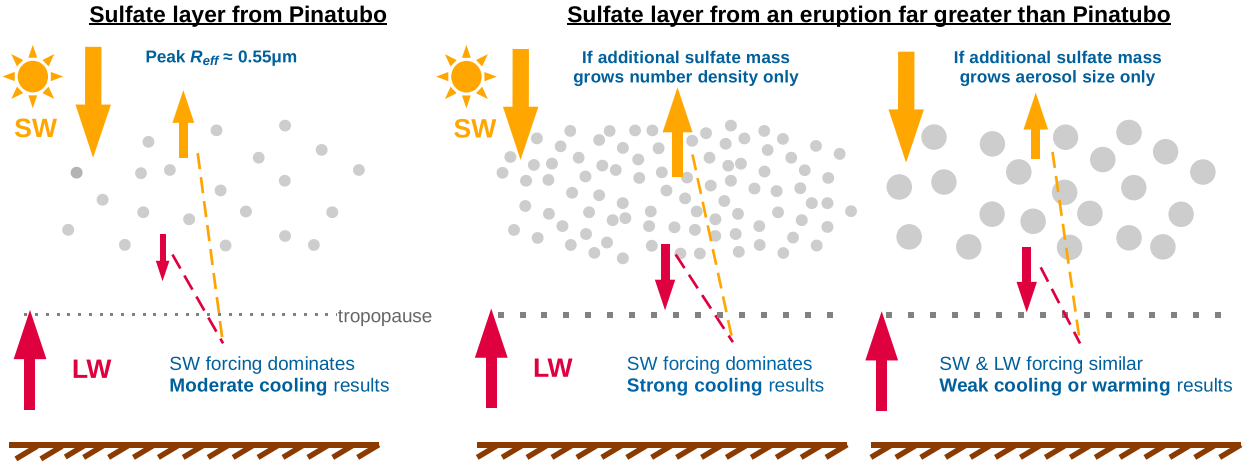

FIG. 4. How sulfate aerosol size influences post-eruption climate. Shown is a schematic demonstrating how sulfate aerosol size affects the surface temperature response to very large eruptions.

size work against this tendency since large aerosol particles are relatively weak scatterers of solar radiation. Sulfate layers concurrently absorb outgoing terrestrial radiation, and this effect also increases with injected mass yet is less sensitive to aerosol size. For larger aerosol sizes, the additional absorption of terrestrial radiation increasingly offsets the additional reflection of solar radiation, and at $R_{\text{eff}} \sim 2\ \mu$m the radiative impact of the absorption fully cancels that of the reflection, as has been demonstrated in Lacis et al. (1992). As injection mass is increased, growth of both shortwave and longwave radiative forcings yields progressively larger sensitivity in net forcing (see Fig. 5a) and temperature response (Fig. 3a) to aerosol size. While both terms become weaker on an efficiency-per-mass basis for more massive eruptions (Fig. 5b), aerosol size controls whether or not the shortwave effect remains dominant. With modest sulfate aerosol sizes, the shortwave forcing leads to surface cooling. Conversely, if sufficiently large aerosol sizes develop, the longwave effect offsets or exceeds the shortwave effect, and weak cooling or even warming can result. We note that none of the interactive aerosol models shown in Fig. 2 attained 2 μm R_{eff}, though one did get close (1.87 μm) and—as described in section 3—these model estimates may not be definitive.

If aerosol size indeed scales with injection mass via a power law, how does the value of k influence super-eruption impacts? In Fig. 6a we show four representative mass-size scalings for eruptions injecting more mass than Pinatubo's 18 Tg SO_2. The peak surface temperature responses from Fig. 3a along these scalings (shown in Fig. 6b) diverge greatly as injected mass is increased, demonstrating the critical need to constrain this scaling. The panels in Fig. 6c show how, among the different scalings, the radiative forcings result in divergent temperature responses as injected mass is increased. For the two weakest growth scalings ($k = 0$ and $k = 1/10$), shortwave forcing continuously dominates. This results in continually stronger cooling up to the 2000 Tg SO_2 mass of the largest evaluated super-eruptions. By comparison, for the scaling with strongest aerosol increase ($k = 1/3$), the positive longwave forcing from sulfate absorbing terrestrial radiation overtakes the shortwave forcing from reflection of solar radiation. This causes a net positive forcing that induces surface warming following the largest super-eruptions. For the $k = 1/4$ scaling, near 300 Tg SO_2 further injection results in equal shortwave and longwave forcing enhancement, preventing larger eruptions from causing significantly more cooling. Note that some mismatch exists between net volcanic aerosol forcing and temperature transitions marking the injection mass where each saturates or reverses. This is partly due to rapid adjustments, which are not included in the shown forcing. A second reason is that the time scale in which the atmosphere thoroughly adjusts to stratospheric aerosol is significant compared to the duration of the peak forcing, rendering top-of-atmosphere forcing a less precise indicator of surface response than it is for a sustained perturbation.

We next evaluate if the assessed aerosol size spread is the likely cause of disagreement among past studies with interactive aerosol models. For this task, we interpolated the peak surface temperature responses from our ModelE simulations to the injected mass and peak global mean aerosol size from several recent interactive aerosol model simulations of large eruptions (Fig. 7, left panel). Accounting for these two values alone (left panel), our model experiments are able to reproduce remarkably similar peak temperature responses as the original studies found. This is in spite of differences in the model used, the simulated eruption season, the injection latitude and height (within the shared criteria of tropical injections into the lower stratosphere), the initial conditions, and inclusion of coinjected species (see Table 1). By comparison, if only the injected masses of the prior studies are used, the peak surface temperature responses cannot be reproduced. Instead of using the peak R_{eff} values in those studies' simulations, we here estimate peak R_{eff} from injected mass according to various power-law scalings (with $k = [0, 1/4, 1/3]$ tested here). In that case, shown in the right column of Fig. 7, prediction is poor regardless of the assumed scaling. Controlling for injection mass, variations in aerosol size thus account for

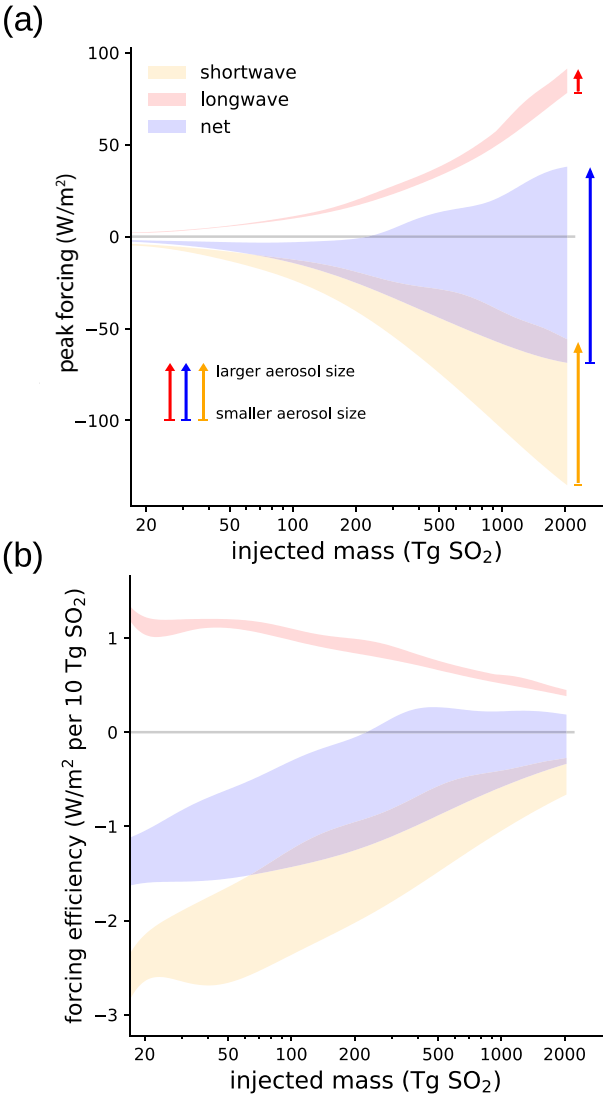

FIG. 5. Radiative forcing uncertainty and eruption mass, showing (a) peak global mean top-of-atmosphere volcanic radiative forcings from the ModelE runs shown in Fig. 3a, covering the range of aerosol sizes and (b) the same data divided by injected mass. The uncertainties at any injection mass are shown as distance across the shaded region. Arrows indicate that larger aerosol particles result in more positive (or less negative) forcings in all cases.

nearly all of the peak temperature response disagreement in previous interactive aerosol model studies of large eruptions. Hence, model disagreement in the temperature response to large SO_2 injections may largely be characterized as disagreement in sulfate aerosol size.

Post-eruption temperature responses in the prior modeling studies cover a large portion of the range found with our ModelE runs (comparing circles to the shaded region in Fig. 3b). However, no previous modeling study has reported global mean warming or weak-to-negligible cooling, as our simulations show could result from super-eruptions that drive strong aerosol growth. Previous studies have included simulations with nearly the maximum theoretical sulfate aerosol size, but not for the most massive eruptions (see Fig. 2). In fact, maximal sulfate aerosol size is a common assumption in simple extrapolations from Pinatubo to larger injection eruptions (Toohey et al. 2016; Crowley and Unterman 2013), including the popular Easy Volcanic Aerosol generator (orange dashed line in Fig. 2). Inputting volcanic sulfate properties based on these extrapolations into a climate model for eruptions larger than Pinatubo thus results in considerably weaker post-eruption cooling than found in the available interactive aerosol model studies. As we will show, strong sulfate growth super-eruption cases cannot readily be deemed unrealistic and hence are worthy of consideration.

5. Post-Toba climate scenarios

Using model simulations, we have shown that a broad range of global surface temperature responses are theoretically possible following a Toba-sized eruption (Fig. 3a). Now we describe three distinct post-Toba scenarios as they appear in our GISS ModelE simulations, and compare the simulated post-eruption climates to records of life in the Toba period and prior model interpretations. The explored scenarios represent strong global mean cooling, moderate cooling, and moderate warming. For this we created three ensembles of a 2000 Tg SO_2 Toba injection, as is most frequently used in Toba modeling studies (Black et al. 2021; Osipov et al. 2020; English et al. 2013), using our ModelE version with prescribed volcanic aerosol (see section 2a). The simulated volcanic sulfate was set to have peak global mean aerosol sizes of R_{eff} = [1.41, 1.79, 2.64] μm across ensembles, as ordered from the most cooling scenario to the warming one (equivalent to extrapolating k = [1/5, 1/4, 1/3] power-law scalings, respectively, from a Pinatubo peak R_{eff} of 0.55 μm at 18 Tg SO_2). As the eruption season is unknown, each ensemble consists of three simulations each for eruptions on 15 January and 15 July (six total for each ensemble).

The resulting surface temperature responses are spatially heterogeneous and starkly dissimilar among scenarios. Depending on sulfate aerosol size, there is pronounced post-eruption cooling or warming over most of Earth's land (Fig. 8a). This includes the northern India and Lake Malawi sites where continuous evidence of life was found across Toba's occurrence (Petraglia et al. 2007; Clarkson et al. 2020; Smith et al. 2018) (see Fig. 8b for local temperature anomalies over time). Over the South African site assessed in Smith et al. (2018) (also in Fig. 8b), only a few months of pronounced warming are found possible and specifically after a winter eruption. However, more robust warming is simulated nearby and over most of southern Africa (see Fig. 8a). Only our peak R_{eff} = 1.41 μm scenario directly disagrees with observations, as it produces post-eruption cooling beyond the estimated 4°C threshold to cause extinction of Lake Malawi biota inconsistent with chemical analyses (Lane et al. 2013). This leaves moderate cooling and moderate warming as consistent with records of life across the Toba eruption.

As in Black et al. (2021), we find that temperature anomalies at the three sites are poorly representative of the global mean response. However, in most of our simulations, post-eruption temperature anomalies at the northern India and

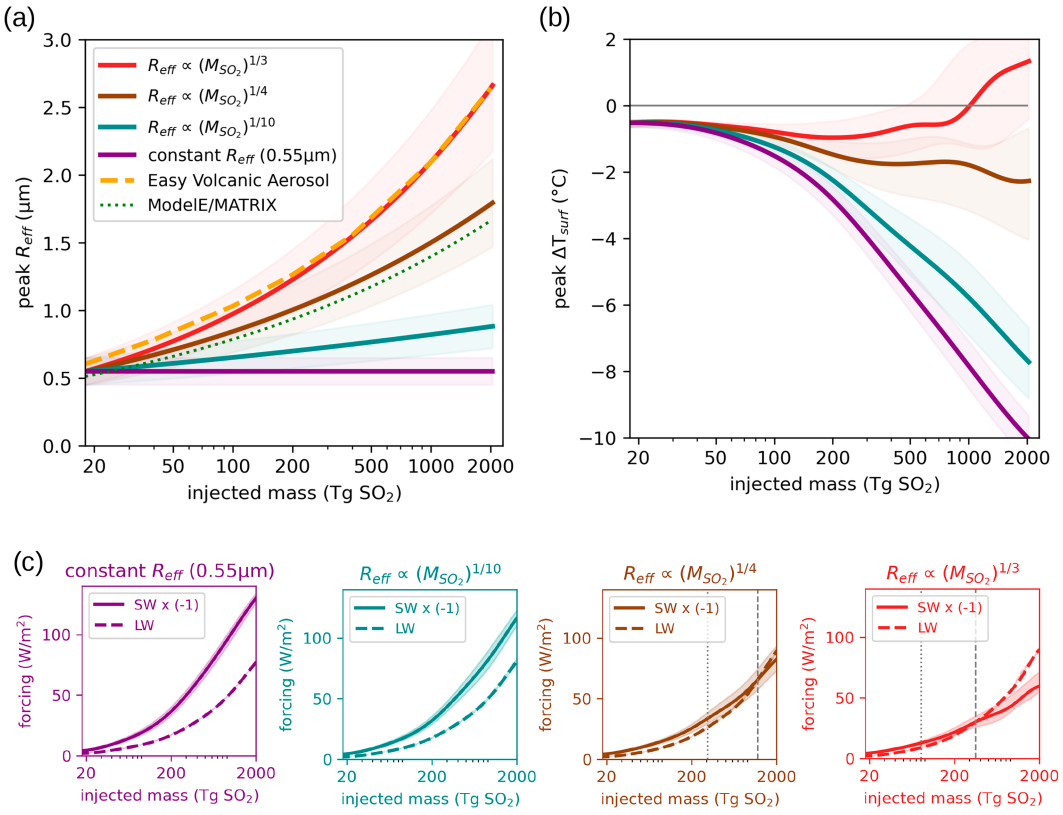

FIG. 6. Ramifications of various injection mass–R_{eff} power-law scalings, showing (a) four dissimilar scalings [via Eq. (1)] stemming from a 0.55 μm peak R_{eff} at 18 Tg SO_2, (b) the resulting global cooling evolution as injected mass is increased, and (c) the longwave (LW) and shortwave (SW) top-of-atmosphere forcings resulting from each scaling. The displayed temperatures and radiative forcings are peak global mean values interpolated from the same ModelE simulations used in Figs. 3a and 6, respectively. Note that (a) also shows the nearest power-law fitting to MATRIX interactive aerosol model output (k = 1/4 from an origin of 0.51 μm at 18 Tg SO_2 and the Easy Volcanic Aerosol (EVA) forcing generator (both as in Fig. 2). Vertical dotted lines in (c) highlight the injected mass where further mass increases strengthen longwave and shortwave forcings equally, while vertical dashed lines indicate masses where longwave and shortwave dominance reverses.

Lake Malawi sites are similar or stronger than on global average for the tested scenarios. This disagrees with Black et al.'s theory that these locations acted as *climate shelters* from global-scale disruption. Our results suggest that climate shelters are not needed to reconcile the extreme cooling found in some modeling studies with their lack of evidence at archaeological and paleoclimate sites. The peak R_{eff} = 1.79 and 2.64 μm ModelE experiments suggest that even for a 2000 Tg SO_2 representation of Toba, modest temperature responses are possible both at the assessed sites and on global average. Further, at inland midlatitude locations like the northern India archaeological site (Fig. 8b), the most potential for cooling was simulated to occur during summer (and warming in winter). This seasonality could have reduced the threat from Toba over these regions regardless of aerosol size scenario.

We emphasize that knowledge from a handful of locations may have limited utility for assessing Toba's widespread impact, as is clear from the preceding discussion. Simulated temperature responses exhibit large spatial heterogeneity, e.g., as our model showed within southern Africa. Hence, records of a single site may poorly represent even regional impacts. Further, the spatial structure disagreement between this study's simulations and those of Black et al. (2021) implies that conclusions on how local responses link to widespread changes will vary strongly depending on the model and experimental setup used, and are hence not robustly known. The available paleoclimate and archaeological records of life across Toba hence have little utility for constraining the post-Toba temperature response. In the next section, we attempt to constrain Toba's response using temperature records of a better constrained but smaller eruption.

6. Constraining super-eruption outcomes with data from the largest Common Era eruption

In this section we evaluate what super-eruption temperature responses are most likely, based on information from two large eruptions of dissimilar magnitude. We first estimate what aerosol size likely followed the largest eruption of the Common Era, that of Mt. Samalas in AD 1257 (Lavigne et al. 2013). Then we

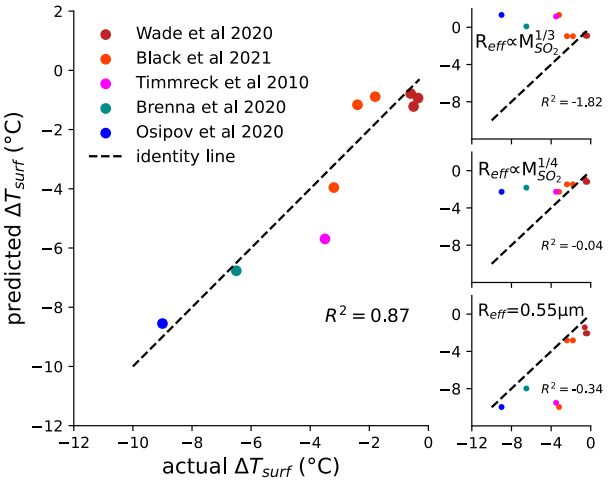

FIG. 7. Reconstructed post-eruption surface temperature responses made by (left) interpolating post-eruption temperatures from ModelE (Fig. 3a) to the injected SO_2 mass and peak sulfate aerosol size of prior studies and (right) using only the injected mass. For the reconstructions using only mass, three simple assumptions on the size of sulfate aerosols are tested: Pinatubo-sized aerosols at all injected masses (peak R_{eff} = 0.55 μm) and two power-law scalings having k = 1/3 and k = 1/4 extrapolated from the 0.55 μm Pinatubo case using Eq. (2). R^2 values less than zero, which are possible when linear interpolation is not the prediction method, indicate poorer predictors than assuming the average among the actual ΔT_{surf}'s in all cases.

use this estimate, along with information on the 1991 Pinatubo eruption, to extrapolate the aerosol size to super-eruption injection masses, and finally we constrain their climate outcomes, as described in sections 6a to 6c. This method yields a new estimate of the likely global mean surface temperature following super-eruptions, and is meant to complement the estimates from site-specific records. The latter, we have argued, are potentially poor indicators of global-scale climate impacts.

a. *Estimating sulfate aerosol size following the AD 1257 Samalas eruption*

We begin by demonstrating that relatively large sulfate aerosol sizes are most compatible with the available data on the Mt. Samalas eruption. This analysis is based on consistency between our ModelE simulations of the Samalas event and the post-Samalas temperatures in the tree ring reconstructions described in section 2c. The tree ring reconstructions cover millennium-length periods during which Samalas is the largest known SO_2 injection, prompting our focus on this eruption.

For our ModelE simulations, we ran a separate five-member ensemble for each of four aerosol size scenarios using prescribed aerosol properties (as described in section 2a). The four simulated post-Samalas aerosol sizes were chosen to span from zero to maximal aerosol size increase with mass, as extrapolated with Eq. (2) from a peak post-Pinatubo R_{eff} of 0.55 μm at 18 Tg SO_2 to Samalas at 120 Tg SO_2, which is near the middle of the estimated 97–140 Tg SO_2 $\pm 1\sigma$ range (Toohey and Sigl 2017). The chosen post-Samalas peak global mean R_{eff} values were 0.55, 0.66, 0.88, and 1.04 μm (equivalent to k = [0, 1/10, 1/4, 1/3], respectively, from this 0.55 μm origin). We set the eruption to occur at the equator in summer (specifically 15 July here), as in previous studies (Wade et al. 2020; Stoffel et al. 2015). We then compared the simulated post-Samalas temperature anomalies to those in the four tree ring records described in section 2c, as shown in Fig. 9a. To best represent the tree ring reconstructions, all temperature values used in this comparison are averages over Northern Hemisphere extratropical land (>40°N) during the summer (JJA) season.

Our comparison shows that the two largest aerosol size ensembles (red and brown vertical bars in Fig. 9a) produce temperature anomalies that are most consistent with the tree ring estimates. Conversely, the two smallest aerosol size cases (teal and purple bars) produced incompatibly strong cooling in our simulations. This suggests that a scaling having strong aerosol size increase with mass (high k) is most able to reconcile the simulated and reconstructed temperatures.

We next systematically estimate the range of global mean peak R_{eff} values that enable simulations to match the temperature anomalies of the tree ring records. Here we simplify our comparison to only evaluating temperature anomalies in the year during which each ensemble or reconstruction has its maximum (hereafter *peak*) anomaly between 1257 and 1261. This enables a straightforward comparison despite a mismatch whereby peak cooling occurs in 1258 in simulations yet a year or two later in most reconstructions, which may reflect a memory lag issue in tree rings (Zhu et al. 2020). We first invert our ModelE results from 1258 (horizontal bars in Fig. 9b, colored as in Fig. 9a) to show which peak post-Samalas temperature anomalies are within each ensemble's bounds. We next construct continuous bounds on aerosol size as a function of temperature anomaly, shown as the gray shaded area in Fig. 9b. This we designed to traverse the model results between quadratic fittings for minimum and maximum aerosol sizes (light gray lines in Fig. 9b). Note that aerosol sizes above 1.22 μm (dashed black line) are not considered, as these would exceed the maximum theoretical aerosol size extrapolated from a Pinatubo mass injection of 18 Tg SO_2 to a Samalas mass of 120 Tg SO_2 [under Eq. (2) with our 0.65 μm high bound on peak Pinatubo R_{eff}].

Averaging the peak post-Samalas temperature anomalies in the four evaluated tree ring reconstructions (black ticks along the horizontal uncertainty bars at the bottom of Fig. 9b) results in a 1.03°C mean post-Samalas cooling over Northern Hemisphere land. Our assessment finds that peak R_{eff} values approximately ranging from 0.86 to 1.22 μm (orange vertical bar in Fig. 9b) can produce consistent cooling as in the ModelE simulations. Further, peak R_{eff} values in excess of 1 μm are compatible with all four assessed tree ring reconstructions. This evaluation indicates that Samalas' large injection mass likely resulted in substantially larger aerosol particles than those from Pinatubo.

b. *Bounding sulfate aerosol size from super-eruptions*

We next use these results to extrapolate sulfate aerosol size to much larger stratospheric SO_2 injections than Samalas. In

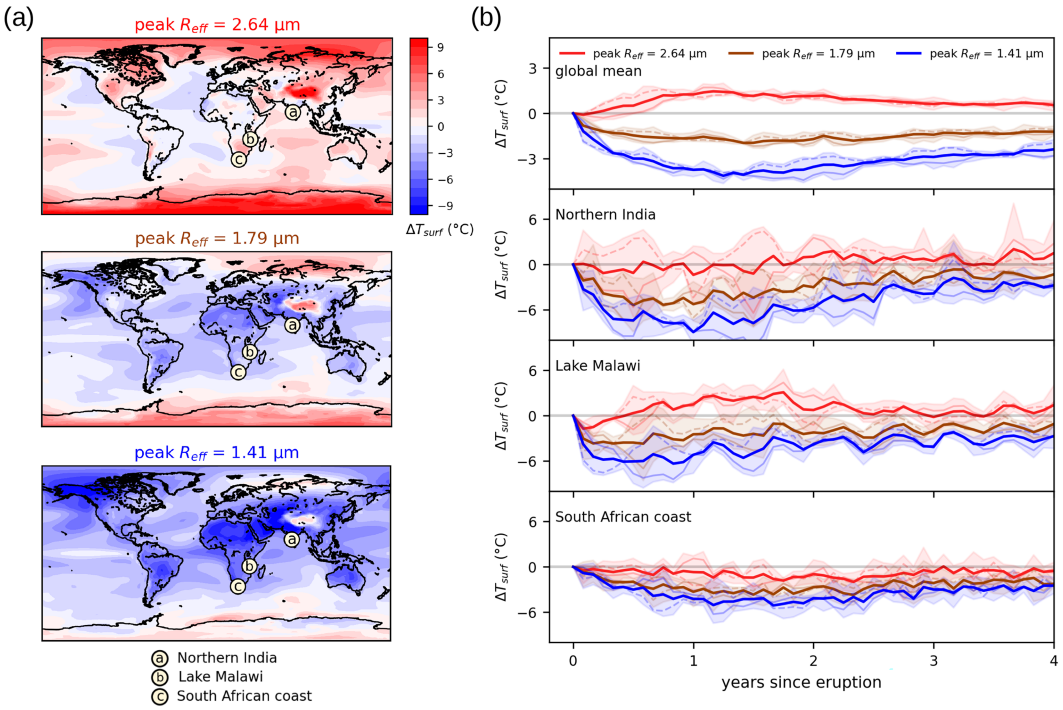

FIG. 8. Simulated temperature responses following three Toba super-eruption scenarios, showing (a) maps of global surface temperature anomalies averaged over the first two post-eruption years and (b) surface temperature evolutions globally and at three sites containing evidence of continuous life across the Toba eruption. The spread among ensemble members is represented in (b) as shaded areas, while faint solid and dashed lines represent averages among January and July eruption members, respectively.

section 3 we had confirmed that extrapolating aerosol size with a power-law scaling [Eq. (1)] is a sound approximation. While direct evidence of super-eruption aerosol size is lacking, this finding suggests that if the sulfate aerosol size following two differently sized volcanic injections is known, super-eruption aerosol size can to first order be estimated by extrapolating to a larger injection mass. Using Pinatubo and Samalas, we therefore now estimate the aerosol size for super-eruptions.

In Fig. 10a, we show four possible scaling curves consistent with both our 0.45–0.65 μm bounds on peak R_{eff} for Pinatubo and our 0.86–1.22 μm bounds for Samalas. The $R_{\text{eff,Pinatubo}}$ and k values that constitute each scaling are presented in Fig. 10a. These four scalings, which encompass the three bounding combinations of the two R_{eff} unknowns (scalings *a*, *b*, and *d*) and the means of both unknowns (scaling *c*), all show substantial increase in aerosol size from Samalas to injections of larger mass. Note that the range of plausible scalings would have been moderately broader if we had tested for a range of Samalas injection masses (e.g., the 97–140 Tg SO_2 $\pm 1\sigma$ ice core uncertainty range) rather than only 120 Tg SO_2. For a 2000 Tg SO_2 super-eruption, looking at the range spanned by our four scalings, one can see that only aerosol sizes larger than 1.3 μm are compatible with the assessed Pinatubo and Samalas evidence. Hence the large sulfate aerosol sizes we find most compatible with Samalas suggest that more massive eruptions result in even larger aerosols.

c. *Constraining the temperature response to super-eruptions*

Last, we use the preceding findings to constrain super-eruption surface temperature responses. Conclusions here are based on an assessment of the four aerosol size scalings in Fig. 10a, which in this panel are shown overlaid on the ModelE global mean temperature response contours from Fig. 3. For clarity the temperature anomaly curves along each scaling are shown in Fig. 10b.

We begin by assessing the plausibility that cooling from super-eruption aerosol is severely limited. As scaling (*b*) traverses the mean of both our Pinatubo and Samalas R_{eff} bounds, we treat this as our best estimate for how aerosol size scales with injection mass. Following the temperature curve in Fig. 10b that results from this scaling, it is evident that simulated cooling increases only up to 200 Tg SO_2 (a black filled circle marks this maximum), beyond which more SO_2 results in *less* volcanic cooling. If this or a scaling producing even larger aerosols (e.g., scaling *a*) were the true scaling, no tropical eruption would be able to cause more than 1°C global mean cooling regardless of injection mass. Further, scalings *a* and *b* raise the possibility that no tropical eruption can cause significantly more cooling than Samalas even if it emits far more SO_2. Note how the cooling for the Samalas eruption (120 Tg SO_2 here) is between the masses of maximum achievable cooling on scalings *a* and *b*, shown as filled black circles. A maximum cooling of even 1.5°C is on the high end of most compatible scalings. Of all scalings that could

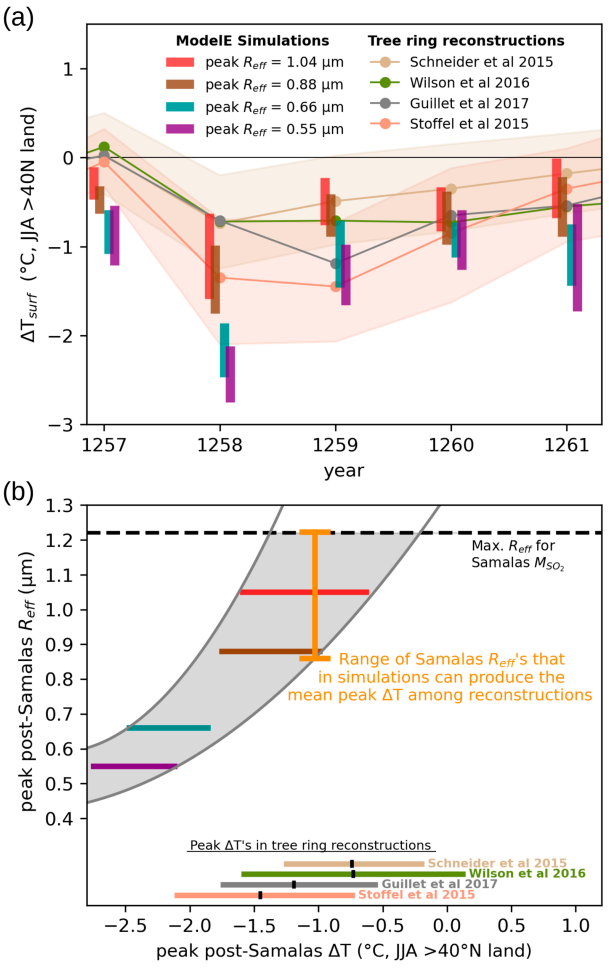

FIG. 9. Comparison between model simulations and tree ring reconstructions of the years following the AD 1257 Samalas eruption. Shown are (a) Northern Hemisphere extratropical land temperatures compared to ModelE simulations of various aerosol size scenarios and (b) estimated peak R_{eff} bounds as a function of simulated post-Samalas temperature anomaly. In (a), the vertical extent of the simulation results (vertical bars) represents the range among ensemble members. In addition to the best-estimate values from four reconstructions (points), we also shown the uncertainty bounds of the Schneider et al. (2015) and Stoffel et al. (2015) reconstructions (tan and salmon shaded regions, respectively). In (b), the estimated range peak R_{eff} values for each potential post-Samalas temperature anomaly is represented by gray shading, with peak post-Samalas temperature anomalies shown at the bottom using best estimates (black ticks) and uncertainty ranges (colored horizontal lines). Figure layout of (a) was based on Fig. 1 of Wade et al. (2020), which we note showed a spline-fit version of the Wilson et al (2016) datset not used here.

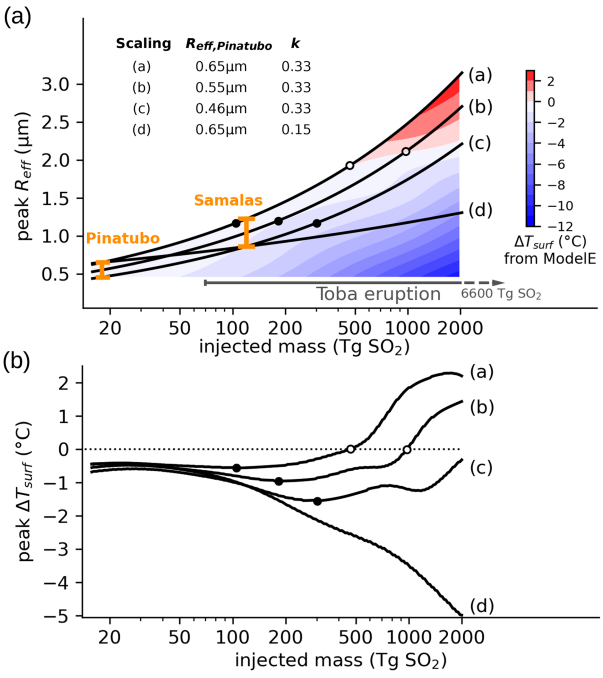

FIG. 10. (a) Four scalings of sulfate aerosol size with mass that are consistent with our bounds on Pinatubo and Samalas peak R_{eff}, shown overlaid on the ModelE global mean temperature responses from Fig. 3a, plus (b) the temperature responses along each scaling. Critical masses of maximum global cooling are marked as filled black circles, while transitions from volcanic cooling to warming are marked with hollow black circles.

possibly link our Pinatubo and Samalas R_{eff} bounds, none results in more than 5°C simulated cooling within the 0–2000 Tg SO_2 assessed injection range, as is demonstrated with scaling (*d*). We hence deem cooling beyond 5°C highly unlikely.

We have shown that volcanic cooling potentially peaks at a finite mass given constraints on sulfate aerosol size. For aerosol size scalings that result in such a critical injection mass, further mass results in less volcanic cooling and may ultimately result in warming. Warming is evident in both scalings *a* and *b* at masses within 1000 Tg SO_2. These transitions from cooling to warming are denoted in Fig. 10 as hollow black circles.

Overall, the magnitude of post-Samalas cooling in tree ring records appears too weak to support the severe super-volcanic cooling hypothesis. The central fit between the Pinatubo and Samalas cases (scaling *b*) could not be extrapolated to a strong cooling outcome at any injection mass, but instead follows the post-eruption scenario of highly limited global cooling, or a warming scenario if mass is sufficiently high and aerosol size > 2 μm can be sustained. Extrapolating data from Pinatubo and Samalas to larger eruptions has required several assumptions, as have been described. We also note that further effort with interactive aerosol models is needed to determine the extent to which each of the presented scalings is realistic. However, the assessment of this section bolsters the credibility of these super-eruption climate scenarios, which in section 4 had been presented as within the physical range of our experiments and in section 5 as unable to be readily falsified by the limited records of life across Toba.

7. Discussion and conclusions

First, our assessment has revealed that a broad range of temperature anomalies following super-eruptions are plausible given the limited available evidence. A large and drastic cooling of the surface is only one of several plausible post-eruption scenarios,

and from our model evaluations appears unlikely. We have demonstrated that uncertainty in the size of sulfate aerosols explains most disagreement among past modeling studies, yet prevents a firm constraint on super-eruption temperature response from being made. Depending on the aerosol size, these eruptions could induce a broad range of climate responses from strong global cooling all the way to warming. We also demonstrated that the available data suggests super-eruption cooling is severely limited, and possibly does not exceed 1.5°C at a critical point beyond which more sulfur mass would reduce this cooling. Moreover, the large sulfate aerosol sizes that result in moderate warming may be possible if super-eruption injection masses are truly on the upper end of estimates and large aerosol particles can be sustained in the stratosphere.

Considering these results, we propose that super-eruptions may pose substantially less of a global threat than has previously been suggested. Our results build on the relatively modest post-Toba cooling estimate of Timmreck et al. (2010). Our simulations indicate that super-eruptions may cause far less cooling than even that study's 3.5°C estimate, no matter how much SO_2 they inject into the stratosphere. At their most severe, the global temperature anomalies posed by super-eruptions would be of similar magnitudes to that from greenhouse gas warming within the next decades, yet of opposite sign and lasting only a few years. However, we also note that if a near-future super-eruption were to inject on the order of 2000 Tg SO_2 into the stratosphere and produce large enough sulfate aerosols to drive a warming response, this might pose an enhanced threat by exacerbating the temperature anomaly from greenhouse gases.

The possibility that sulfate from super-eruptions could drive global mean warming may be worth further consideration, as this scenario cannot be ruled out with current evidence. Its potential occurrence expands the possible explanations for paleoclimate and archaeological findings: for instance, it could explain the evidence of a lasting technological advance in southern Africa following Toba (Smith et al. 2018; Brown et al. 2012). Given our findings, this could be interpreted not only as humans adapting to a threat from cooling (Smith et al. 2018), but possibly to the harm or benefits from warming in parts of the region. although we have focused only on surface temperature shifts, other perceived global threats of super-eruptions could potentially be beneficial or at least inflict little harm. An example is that while super-eruptions might be perceived as a threat to food supplies by blocking sunlight used in photosynthesis, Pinatubo's eruption was actually found to enhance photosynthesis through the benefits of diffuse light (Gu et al. 2003). Thus, it could be worthwhile to reassess the overall global-scale threat posed by large volcanic eruptions.

Although we have focused specifically on uncertainty in peak global mean aerosol size, this is itself a product of uncertainties in microphysics, chemistry, and dynamics. There also exist additional uncertainties that could reduce confidence in temperature response estimates. Uncertainty in super-eruption SO_2 mass remains a major issue. Post-eruption warming might be more prominent if we had tested for Toba injecting more than 2000 Tg of stratospheric SO_2, as multiple injection mass estimates indicate is possible (Costa et al. 2014; Zielinski et al. 1996). We note that ice core analysis may underestimate erupted mass due to sedimentation of large sulfate aerosols prior to reaching ice core locations, as these estimates use simple scalings based on more modest eruptions that produce smaller, more readily transported aerosols. Our surface temperature response bounds would also likely be larger if we had accounted for such unknowns as sulfate aerosol composition or aerosol size heterogeneity. Conversely, the available simulations with interactive aerosol microphysics—including our own with ModelE/MATRIX—support a narrower range than our prescribed aerosol experiments and did not attain sufficiently large aerosols for warming.

Important caveats should be noted regarding our use of simulations lacking interactive microphysics and chemistry for assessing surface temperature impacts. Our prescribed aerosol experiments with ModelE did not scale aerosol extinction values to account for larger aerosol sizes causing sulfate to gravitationally settle faster than during Pinatubo. That sedimentation strengthens with aerosol size (Pinto et al. 1989) could narrow the physically sustainable range of aerosol sizes to less than examined here, reducing the plausibility of aerosol-induced warming. An interactive representation of gravitational sedimentation could also shorten the estimated duration of peak effective radius, as well as that of the temperature anomalies resulting from sulfate's presence in the stratosphere. These simulations also did not explicitly include eruption impacts on stratospheric OH, which influences the chemical formation rate of volcanic sulfate (Pinto et al. 1989). Eruptions can either deplete (Pinto et al. 1989) or augment (Zhu et al. 2022) stratospheric OH supply, but this depends on the amount of co-emitted water vapor, which is unknown following super-eruptions. Despite these omissions, we were able to effectively estimate the global mean peak temperature responses from contemporary interactive aerosol models using the simpler prescribed aerosol setup (cf. Fig. 7). However, we encourage further use of interactive aerosol models to test whether larger sulfate particles can survive in the stratosphere for a climate-relevant duration. For this to be possible, large aerosol particles would need to be sustained in the tropical stratosphere for a duration of months without being removed by poleward transport or gravitational settling. Currently, models heavily disagree in the relevant circulation strengths, which may account for part of their inability to agree on volcanic aerosol size (Aubry et al. 2021; Timmreck et al. 2018). To more rigorously constrain aerosol size than we have done here, one way forward would be to develop a comprehensive super-eruption model intercomparison project (MIP). Such a MIP would replicate identical super-eruption scenarios—such as Toba for both low and high sulfur mass estimates—in several Earth system models with interactive microphysics and chemistry, mirroring past experiments involving smaller eruptions (Clyne et al. 2021; Timmreck et al. 2018). Until a more concerted effort is made to constrain super-eruption aerosol size, we recommend that prescribed aerosol experiments use not only the maximal scaling factor of $k = 1/3$, as is currently standard, but additionally test a lower aerosol size scenario such as the $k = 1/4$ scaling we found to be supported by ModelE/MATRIX. We additionally express caution in prescribing R_{eff} values above 2 μm, as it has not been established that such aerosols can be sustained in the stratosphere.

Our findings highlight that attempts to attribute large-scale destruction of societies and ecosystems to rare volcanic

eruptions through the bottom-up approach of modeling tend to be simplistic and highly speculative. Records of life across the Toba eruption offer more direct evidence of whether extreme climate disruption has occurred, yet are of limited quantitative utility and do not confidently represent changes over wider regions. Along with improved estimates of SO_2 injection mass, a deeper understanding of the factors determining volcanic aerosol size may be the most promising path to constraining the climate impacts of Toba and other super-eruptions. This could potentially be achieved through a mix of laboratory and model experiments of dense sulfate layers under stratospheric conditions. One avenue would be additional interactive aerosol simulations exploring how aerosol size scales with injection mass, as we tested here with ModelE/MATRIX but exploring pertinent sensitivities in microphysics, chemistry, and dynamics. Until considerable progress is made, surface temperature responses to very large eruptions will remain poorly constrained, and model-based estimates of their impacts should therefore be communicated as having considerable uncertainty.

Acknowledgments. L. M. P. and K. D. were funded by Grant 1914579 from the U.S. National Science Foundation to Columbia University. The development of GISS ModelE at NASA GISS is supported by the NASA Modeling, Analysis, and Prediction (MAP) Program. Resources supporting this work were provided by the NASA High-End Computing (HEC) Program through the NASA Center for Climate Simulation (NCCS) at Goddard Space Flight Center.

Data availability statement. GISS ModelE output used in this study's analysis and figures has been deposited in a Zenodo archive (https://doi.org/10.5281/zenodo.7083247).

REFERENCES

Ambrose, S. H., 1998: Late Pleistocene human population bottlenecks, volcanic winter, and differentiation of modern humans. *J. Hum. Evol.*, **34**, 623–651, https://doi.org/10.1006/jhev.1998.0219.

Aubry, T. J., M. Toohey, L. Marshall, A. Schmidt, and A. M. Jellinek, 2020: A new volcanic stratospheric sulfate aerosol forcing emulator (EVA_H): Comparison with interactive stratospheric aerosol models. *J. Geophys. Res. Atmos.*, **125**, e2019JD031303, https://doi.org/10.1029/2019JD031303.

——, J. Staunton-Sykes, L. R. Marshall, J. Haywood, N. L. Abraham, and A. Schmidt, 2021: Climate change modulates the stratospheric volcanic sulfate aerosol lifecycle and radiative forcing from tropical eruptions. *Nat. Commun.*, **12**, 4708, https://doi.org/10.1038/s41467-021-24943-7.

Bauer, S. E., D. L. Wright, D. Koch, E. R. Lewis, R. McGraw, L.-S. Chang, S. E. Schwartz, and R. Ruedy, 2008: MATRIX (Multiconfiguration Aerosol TRacker of mIXing state): An aerosol microphysical module for global atmospheric models. *Atmos. Chem. Phys.*, **8**, 6003–6035, https://doi.org/10.5194/acp-8-6003-2008.

——, and Coauthors, 2020: Historical (1850–2014) aerosol evolution and role on climate forcing using the GISS ModelE2.1 contribution to CMIP6. *J. Adv. Model. Earth Syst.*, **12**, e2019MS001978, https://doi.org/10.1029/2019MS001978.

Bingen, C., D. Fussen, and F. Vanhellemont, 2004: A global climatology of stratospheric aerosol size distribution parameters derived from SAGE II data over the period 1984–2000: 1. Methodology and climatological observations. *J. Geophys. Res.*, **109**, D06201, https://doi.org/10.1029/2003JD003518.

Black, B. A., J.-F. Lamarque, D. R. Marsh, A. Schmidt, and C. G. Bardeen, 2021: Global climate disruption and regional climate shelters after the Toba supereruption. *Proc. Natl. Acad. Sci. USA*, **118**, e2013046118, https://doi.org/10.1073/pnas.2013046118.

Brenna, H., S. Kutterolf, M. J. Mills, and K. Krüger, 2020: The potential impacts of a sulfur- and halogen-rich supereruption such as Los Chocoyos on the atmosphere and climate. *Atmos. Chem. Phys.*, **20**, 6521–6539, https://doi.org/10.5194/acp-20-6521-2020.

Brown, K. S., and Coauthors, 2012: An early and enduring advanced technology originating 71,000 years ago in South Africa. *Nature*, **491**, 590–593, https://doi.org/10.1038/nature11660.

Chan, T. W., and M. Mozurkewich, 2001: Measurement of the coagulation rate constant for sulfuric acid particles as a function of particle size using tandem differential mobility analysis. *J. Aerosol Sci.*, **32**, 321–339, https://doi.org/10.1016/S0021-8502(00)00081-1.

Clarkson, C., and Coauthors, 2020: Human occupation of northern India spans the Toba super-eruption ~74,000 years ago. *Nat. Commun.*, **11**, 961, https://doi.org/10.1038/s41467-020-14668-4.

Clyne, M., and Coauthors, 2021: Model physics and chemistry causing intermodel disagreement within the VolMIP-Tambora interactive stratospheric aerosol ensemble. *Atmos. Chem. Phys.*, **21**, 3317–3343, https://doi.org/10.5194/acp-21-3317-2021.

Costa, A., V. C. Smith, G. Macedonio, and N. E. Matthews, 2014: The magnitude and impact of the youngest Toba tuff supereruption. *Front. Earth Sci.*, **2**, 16, https://doi.org/10.3389/feart.2014.00016.

Crick, L., and Coauthors, 2021: New insights into the ~74 ka Toba eruption from sulfur isotopes of polar ice cores. *Climate Past*, **17**, 2119–2137, https://doi.org/10.5194/cp-17-2119-2021.

Crowley, T. J., and M. B. Unterman, 2013: Technical details concerning development of a 1200 yr proxy index for global volcanism. *Earth Syst. Sci. Data*, **5**, 187–197, https://doi.org/10.5194/essd-5-187-2013.

DallaSanta, K., and L. M. Polvani, 2022: Volcanic stratospheric injections up to 160 Tg(S) yield a Eurasian winter warming indistinguishable from internal variability. *Atmos. Chem. Phys.*, **22**, 8843–8862, https://doi.org/10.5194/acp-22-8843-2022.

Deshler, T., 1994: In situ measurements of Pinatubo aerosol over Kiruna on four days between 18 January and 13 February 1992. *Geophys. Res. Lett.*, **21**, 1323–1326, https://doi.org/10.1029/93GL03227.

——, J. B. Liley, G. Bodeker, W. A. Matthews, and D. J. Hoffmann, 1997: Stratospheric aerosol following Pinatubo, comparison of the north and south mid latitudes using in situ measurements. *Adv. Space Res.*, **20**, 2089–2095, https://doi.org/10.1016/S0273-1177(97)00600-5.

English, J. M., O. B. Toon, and M. J. Mills, 2013: Microphysical simulations of large volcanic eruptions: Pinatubo and Toba. *J. Geophys. Res. Atmos.*, **118**, 1880–1895, https://doi.org/10.1002/jgrd.50196.

Goodman, J., K. G. Snetsinger, R. F. Pueschel, G. V. Ferry, and S. Verma, 1994: Evolution of Pinatubo aerosol near 19 km altitude over western North America. *Geophys. Res. Lett.*, **21**, 1129–1132, https://doi.org/10.1029/94GL00696.

Gu, L., D. D. Baldocchi, S. C. Wofsy, J. W. Munger, J. J. Michalsky, S. P. Urbanski, and T. A. Boden, 2003: Response of a

deciduous forest to the Mount Pinatubo eruption: Enhanced photosynthesis. *Science*, **299**, 2035–2038, https://doi.org/10.1126/science.1078366.

Guillet, S., and Coauthors, 2017: Climate response to the Samalas volcanic eruption in 1257 revealed by proxy records. *Nat. Geosci.*, **10**, 123–128, https://doi.org/10.1038/ngeo2875.

Guo, S., G. J. S. Bluth, W. I. Rose, I. M. Watson, and A. J. Prata, 2004: Re-evaluation of SO_2 release of the 15 June 1991 Pinatubo eruption using ultraviolet and infrared satellite sensors. *Geochem. Geophys. Geosyst.*, **5**, Q04001, https://doi.org/10.1029/2003GC000654.

Hansen, J. E., and L. D. Travis, 1974: Light scattering in planetary atmospheres. *Space Sci. Rev.*, **16**, 527–610, https://doi.org/10.1007/BF00168069.

IACETH, 2017: CMIP6 Stratospheric Aerosol Dataset (SAD) v3. Institute for Atmosphere and Climate, ETH Zurich, Earth System Grid Federation, accessed 1 December 2022, https://doi.org/10.22033/ESGF/input4MIPs.1681.

Kremser, S., and Coauthors, 2016: Stratospheric aerosol—Observations, processes, and impact on climate. *Rev. Geophys.*, **54**, 278–335, https://doi.org/10.1002/2015RG000511.

Lacis, A., J. Hansen, and M. Sato, 1992: Climate forcing by stratospheric aerosols. *Geophys. Res. Lett.*, **19**, 1607–1610, https://doi.org/10.1029/92GL01620.

Lane, C. S., B. T. Chorn, and T. C. Johnson, 2013: Ash from the Toba supereruption in Lake Malawi shows no volcanic winter in East Africa at 75 ka. *Proc. Natl. Acad. Sci. USA*, **110**, 8025–8029, https://doi.org/10.1073/pnas.1301474110.

Lavigne, F., and Coauthors, 2013: Source of the great A.D. 1257 mystery eruption unveiled, Samalas volcano, Rinjani volcanic complex, Indonesia. *Proc. Natl. Acad. Sci. USA*, **110**, 16 742–16 747, https://doi.org/10.1073/pnas.1307520110.

Manning, J. G., F. Ludlow, A. R. Stine, W. R. Boos, M. Sigl, and J. R. Marlon, 2017: Volcanic suppression of Nile summer flooding triggers revolt and constrains interstate conflict in ancient Egypt. *Nat. Commun.*, **8**, 900, https://doi.org/10.1038/s41467-017-00957-y.

McConnell, J. R., and Coauthors, 2020: Extreme climate after massive eruption of Alaska's Okmok volcano in 43 BCE and effects on the late Roman Republic and Ptolemaic Kingdom. *Proc. Natl. Acad. Sci. USA*, **117**, 15 443–15 449, https://doi.org/10.1073/pnas.2002722117.

Mills, M. J., and Coauthors, 2016: Global volcanic aerosol properties derived from emissions, 1990–2014, using CESM1 (WACCM). *J. Geophys. Res. Atmos.*, **121**, 2332–2348, https://doi.org/10.1002/2015JD024290.

Orbe, C., and Coauthors, 2020: GISS Model E2.2: A climate model optimized for the middle atmosphere—2. Validation of large-scale transport and evaluation of climate response. *J. Geophys. Res. Atmos.*, **125**, e2020JD033151, https://doi.org/10.1029/2020JD033151.

Osipov, S., G. Stenchikov, K. Tsigaridis, A. N. LeGrande, and S. E. Bauer, 2020: The role of the SO_2 radiative effect in sustaining the volcanic winter and soothing the Toba impact on climate. *J. Geophys. Res. Atmos.*, **125**, e2019JD031726, https://doi.org/10.1029/2019JD031726.

Petraglia, M., and Coauthors, 2007: Middle Paleolithic assemblages from the Indian subcontinent before and after the Toba super-eruption. *Science*, **317**, 114–116, https://doi.org/10.1126/science.1141564.

Pinto, J. P., R. P. Turco, and O. B. Toon, 1989: Self-limiting physical and chemical effects in volcanic eruption clouds. *J. Geophys. Res.*, **94**, 11 165–11 174, https://doi.org/10.1029/JD094iD08p11165.

Pueschel, R. F., P. B. Russell, D. A. Allen, G. V. Ferry, K. G. Snetsinger, J. M. Livingston, and S. Verma, 1994: Physical and optical properties of the Pinatubo volcanic aerosol: Aircraft observations with impactors and a sun-tracking photometer. *J. Geophys. Res.*, **99**, 12 915–12 922, https://doi.org/10.1029/94JD00621.

Rampino, M. R., and S. Self, 1992: Volcanic winter and accelerated glaciation following the Toba super-eruption. *Nature*, **359**, 50–52, https://doi.org/10.1038/359050a0.

——, and S. H. Ambrose, 2000: Volcanic winter in the Garden of Eden: The Toba super-eruption and the late Pleistocene human population crash. *Volcanic Hazards and Disasters in Human Antiquity*, F. W. McCoy and G. Heiken, Eds., Special Paper 345, Geological Society of America, 71–82.

Rind, D., and Coauthors, 2020: GISS Model E2.2: A climate model optimized for the middle atmosphere—Model structure, climatology, variability, and climate sensitivity. *J. Geophys. Res. Atmos.*, **125**, e2019JD032204, https://doi.org/10.1029/2019JD032204.

Robock, A., C. M. Ammann, L. Oman, D. Shindell, S. Levis, and G. Stenchikov, 2009: Did the Toba volcanic eruption of ~74 ka B.P. produce widespread glaciation? *J. Geophys. Res.*, **114**, D10107, https://doi.org/10.1029/2008JD011652.

Sato, M., J. E. Hansen, A. Lacis, M. P. McCormick, J. B. Pollack, L. Thomason, and A. Bourassa, 2012: Stratospheric aerosol optical thickness in the GISS climate model. NASA, accessed 1 December 2022, https://data.giss.nasa.gov/modelforce/strataer/.

Schneider, L., J. E. Smerdon, U. Büntgen, R. J. S. Wilson, V. S. Myglan, A. V. Kirdyanov, and J. Esper, 2015: Revising mid-latitude summer temperatures back to A.D. 600 based on a wood density network. *Geophys. Res. Lett.*, **42**, 4556–4562, https://doi.org/10.1002/2015GL063956.

Sekiya, T., K. Sudo, and T. Nagai, 2016: Evolution of stratospheric sulfate aerosol from the 1991 Pinatubo eruption: Roles of aerosol microphysical processes. *J. Geophys. Res. Atmos.*, **121**, 2911–2938, https://doi.org/10.1002/2015JD024313.

Sioris, C. E., A. Malo, C. A. McLinden, and R. D'Amours, 2016: Direct injection of water vapor into the stratosphere by volcanic eruptions. *Geophys. Res. Lett.*, **43**, 7694–7700, https://doi.org/10.1002/2016GL069918.

Smith, E. I., and Coauthors, 2018: Humans thrived in South Africa through the Toba eruption about 74,000 years ago. *Nature*, **555**, 511–515, https://doi.org/10.1038/nature25967.

Stoffel, M., and Coauthors, 2015: Estimates of volcanic-induced cooling in the Northern Hemisphere over the past 1,500 years. *Nat. Geosci.*, **8**, 784–788, https://doi.org/10.1038/ngeo2526.

Svensson, A., and Coauthors, 2013: Direct linking of Greenland and Antarctic ice cores at the Toba eruption (74 ka BP). *Climate Past*, **9**, 749–766, https://doi.org/10.5194/cp-9-749-2013.

Thomason, L. W., 1992: Observations of a new SAGE II aerosol extinction mode following the eruption of Mt. Pinatubo. *Geophys. Res. Lett.*, **19**, 2179–2182, https://doi.org/10.1029/92GL02185.

Timmreck, C., H.-F. Graf, S. J. Lorenz, U. Niemeier, D. Zanchettin, D. Matei, J. H. Jungclaus, and T. J. Crowley, 2010: Aerosol size confines climate response to volcanic super-eruptions. *Geophys. Res. Lett.*, **37**, L24705, https://doi.org/10.1029/2010GL045464.

——, and Coauthors, 2018: The Interactive Stratospheric Aerosol Model Intercomparison Project (ISA-MIP): Motivation and experimental design. *Geosci. Model Dev.*, **11**, 2581–2608, https://doi.org/10.5194/gmd-11-2581-2018.

Toohey, M., and M. Sigl, 2017: Volcanic stratospheric sulfur injections and aerosol optical depth from 500 BCE to 1900 CE.

Earth Syst. Sci. Data, **9**, 809–831, https://doi.org/10.5194/essd-9-809-2017.

——, B. Stevens, H. Schmidt, and C. Timmreck, 2016: Easy Volcanic Aerosol (EVA v1.0): An idealized forcing generator for climate simulations. *Geosci. Model Dev.*, **9**, 4049–4070, https://doi.org/10.5194/gmd-9-4049-2016.

Ukhov, A., G. Stenchikov, S. Osipov, N. Krotkov, N. Gorkavyi, C. Li, O. Dubovik, and A. Lopatin, 2023: Inverse modeling of the initial stage of the 1991 Pinatubo volcanic cloud accounting for radiative feedback of volcanic ash. *J. Geophys. Res. Atmos.*, **128**, e2022JD038446, https://doi.org/10.1029/2022JD038446.

Vandergoes, M. J., and Coauthors, 2013: A revised age for the Kawakawa/Oruanui tephra, a key marker for the last glacial maximum in New Zealand. *Quat. Sci. Rev.*, **74**, 195–201, https://doi.org/10.1016/j.quascirev.2012.11.006.

Wade, D. C., and Coauthors, 2020: Reconciling the climate and ozone response to the 1257 CE Mount Samalas eruption. *Proc. Natl. Acad. Sci. USA*, **117**, 26 651–26 659, https://doi.org/10.1073/pnas.1919807117.

Wilson, J. C., and Coauthors, 1993: In situ observations of aerosol and chlorine monoxide after the 1991 eruption of Mount Pinatubo: Effect of reactions on sulfate aerosol. *Science*, **261**, 1140–1143, https://doi.org/10.1126/science.261.5125.1140.

Wilson, R., and Coauthors, 2016: Last millennium Northern Hemisphere summer temperatures from tree rings: Part I: The long term context. *Quat. Sci. Rev.*, **134**, 1–18, https://doi.org/10.1016/j.quascirev.2015.12.005.

Yost, C. L., L. J. Jackson, J. R. Stone, and A. S. Cohen, 2018: Subdecadal phytolith and charcoal records from Lake Malawi, East Africa imply minimal effects on human evolution from the ~74 ka Toba supereruption. *J. Hum. Evol.*, **116**, 75–94, https://doi.org/10.1016/j.jhevol.2017.11.005.

Zanchettin, D., and Coauthors, 2016: The model intercomparison project on the climatic response to volcanic forcing (VolMIP): Experimental design and forcing input data for CMIP6. *Geosci. Model Dev.*, **9**, 2701–2719, https://doi.org/10.5194/gmd-9-2701-2016.

——, and Coauthors, 2022: Effects of forcing differences and initial conditions on inter-model agreement in the VolMIP volc-Pinatubo-full experiment. *Geosci. Model Dev.*, **15**, 2265–2292, https://doi.org/10.5194/gmd-15-2265-2022.

Zhu, F., J. Emile-Geay, G. J. Hakim, J. King, and K. J. Anchukaitis, 2020: Resolving the differences in the simulated and reconstructed temperature response to volcanism. *Geophys. Res. Lett.*, **47**, e2019GL086908, https://doi.org/10.1029/2019GL086908.

Zhu, Y., and Coauthors, 2022: Perturbations in stratospheric aerosol evolution due to the water-rich plume of the 2022 Hunga-Tonga eruption. *Commun. Earth Environ.*, **3**, 248, https://doi.org/10.1038/s43247-022-00580-w.

Zielinski, G. A., P. A. Mayewski, L. D. Meeker, S. Whitlow, M. S. Twickler, and K. Taylor, 1996: Potential atmospheric impact of the Toba mega-eruption ~71,000 years ago. *Geophys. Res. Lett.*, **23**, 837–840, https://doi.org/10.1029/96GL00706.